Li *et al. Carbon Research* (2024) 3:4
https://doi.org/10.1007/s44246-023-00085-x

Carbon Research

ORIGINAL ARTICLE

Open Access

Properties and photosynthetic promotion mechanisms of artificial humic acid are feedstock-dependent

Xiaona Li[1,2], Yancai Zhi[1], Minghao Jia[1], Xiaowei Wang[1], Mengna Tao[1], Zhenyu Wang[1,2,3*] and Baoshan Xing[4]

Abstract

The artificial humic acids (AHA) approach contributes to achieving the carbon (C) emission peaking and neutrality goal through efficient recycling of waste biomasses and promotion of plant photosynthesis. However, the dependence of their production processes and photosynthetic promotion mechanisms on feedstocks remains unclear. In this study, waste biomasses including camphor leaves (CL), corn stalks (CS), peanut shells (PS), and mixed cyanobacteria (MC) have been respectively converted into artificial humic acids through an environmentally friendly hydrothermal humification approach. The dynamic humification process of different feedstocks and the composition, structural properties, and electron transfer capacity of AHA products were determined. Moreover, the different AHA products were applied to corn to explore their respective photosynthetic promotion mechanisms. High relative contents of lignin and C/N in feedstocks are not conducive to the formation of photodegradable substances and the redox property in AHA. The application of AHA increased the net photosynthetic rate and biomass C of corn by 70–118% and 22–39%, respectively. The AHA produced from higher H/C (0.19) and hemicellulose content (17.09%) in feedstocks (e.g., MC) increased corn photosynthesis by improving light energy capture and conversion efficiency in the PSII process. In contrast, the AHA produced from a higher content of lignin (19.81%) and C/N (7.67) in feedstocks (e.g., CS) increased corn photosynthesis by providing functional enzymes (proteins) and nutrients for leaves. This work provides new insights into the utilization of renewable resources, and the artificial humic acids approach sheds light on environmental sustainability by constructing a closed loop of C in environments.

Highlights

- AHA benefits carbon neutrality by C loss reduction and photosynthesis promotion.
- AHA properties depend on lignin content and C/N of feedstocks.
- Photosynthetic promotion mechanisms of AHA are feedstock-dependent.
- AHA_{MC} increases light capture and conversion efficiency to improve photosynthesis.
- AHA_{CS} provides functional enzymes and nutrients to improve photosynthesis.

Keywords Carbon neutrality, Feedstock property, Hydrothermal humification, Photosynthetic mechanisms, Renewable resource

Handling Editor: Fangbai Li

*Correspondence:
Zhenyu Wang
wang0628@jiangnan.edu.cn
Full list of author information is available at the end of the article

Graphical Abstract

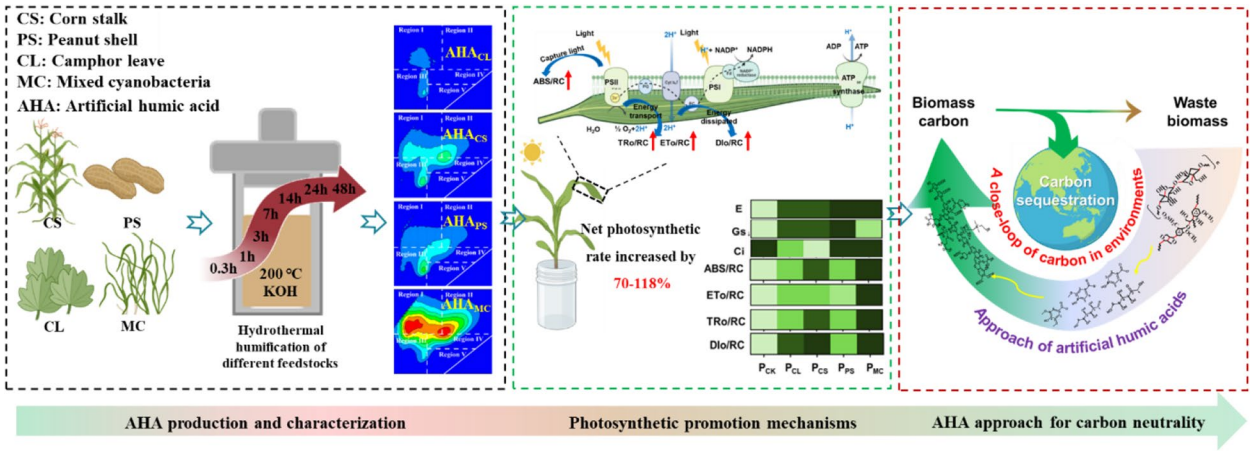

1 Introduction

Humic acids, accounting for about 80% of the soil organic matter, are regarded as the key to soil health (Shen et al. 2021; Yang and Antonietti 2020a). However, the formation of natural humic acids includes complex microbial and chemical reactions and requires quite a long time in strict environmental conditions (Yang and Antonietti 2020b). Therefore, the majority of soils are in deficiency of humic acids. Peatlands, which are rich in natural humic acids, cover only less than 3% of Earth's lands (Dargie et al. 2017). Therefore, pure chemical lab synthesis of artificial humic acids, a kind of advanced polymer materials, has recently been developed for soil improvement (Yang and Antonietti 2020a, 2020b). Green synthesis of artificial humic acids from waste biomasses reduces carbon dioxide (CO_2) emissions from their natural decomposition, benefiting the effort to tackle the climate crisis by reducing C loss and creating a sustainable environment. Moreover, the application of artificial humic acids improves C and nutrients fixation, and thus conducive to soil fertility and plant growth.

Hydrothermal humification has received significant attention for producing artificial humic acids since it is both environmentally and economically friendly (Yang et al. 2021). During the hydrothermal humification process, a trace amount of CO_2 is released (Manasrah et al. 2020). Moreover, compared with incineration, converting straw in each hectare of farmland into artificial humic acids brings about $20.4 benefits (Zhi et al. 2022). During hydrothermal humification under an alkaline solution, macromolecular biomass is firstly decomposed by radicals such as •OH into various monomers and then condensed into artificial humic acids (Vardon et al. 2015). Compared to cellulose, lignin decomposition is more difficult due to its recalcitrant alkyl-aromatic structure (Shen et al. 2021; Wu et al. 2020). Lignin can be hydrolyzed into aromatic monomers for subsequent condensation; In contrast, cellulose decomposition mainly produces aliphatic monomers such as glucose (Kamimura et al. 2019; Ralph et al. 2019; Fig. S1). The composition of various monomers determines the composition and structure of artificial humic acids (Yang et al. 2019; Zhi et al. 2022). For example, aromatic monomers play an important role in the electrophilic substitution reactions of artificial humic acids. In addition, the ratio of C to nitrogen (C/N) in feedstocks determines the humification efficiency and nutrient contents in humic acids (Shen et al. 2021). Therefore, the properties of artificial humic acids are likely to be feedstock-dependent.

Artificial humic acids show great potential in promoting plant photosynthesis. Due to the strong redox properties, artificial humic acids promote light energy capture and electron transfer of organisms (Zhang et al. 2020). Certain compositions such as coumaric acid and isocitrate in artificial humic acids upregulate the expression of OsDCL to promote chlorophyll synthesis in plants (Zhang et al. 2020). The catechol and protocatechol in artificial humic acids can increase energy metabolism (e.g., tricarboxylic acid cycle) in plants (Kamimura et al. 2019; Vardon et al. 2015). The nitrogen uptake of crops can also be stimulated by artificial humic acids, benefiting the intercellular diffusion and assimilation of CO_2 and promoting the photosynthetic C fixation of plants (Huang et al. 2022). Generally, plant photosynthesis can be improved via the following three mechanisms: 1) increasing light energy capture capacity, 2) increasing

light energy conversion efficiency in Photosystem II (PSII) process, and 3) increasing nitrogen content in plant leaves (Huang et al. 2022). The mechanisms of different artificial humic acids in promoting photosynthesis have not been well understood, which limits their specific applications in environments. We hypothesize that a higher content of lignin in feedstocks leads to a slower hydrothermal humification process, and the produced artificial humic acids could mainly improve the light energy capture ability and light energy conversion efficiency in the PSII process of plants; the feedstocks with lower C/N can conduct thorough hydrothermal humification processes, and the artificial humic acids products may promote photosynthesis by providing more N for CO_2 assimilation in plants.

To test our hypotheses, four types of waste biomass including camphor leaves (CL), corn stalks (CS), peanut shells (PS), and mixed cyanobacteria (MC), which have varied C structures and lignocellulose properties, were chosen for hydrothermal synthesis of artificial humic acids. The dynamic humification process of feedstocks was examined and the composition, structural properties, and electron transfer capacity (ECT) of artificial humic acids were determined. Furthermore, the produced artificial humic acids were applied for promoting corn photosynthesis and exploring the associated mechanisms in correlation networks. Considering both decreases in the natural decomposition of waste biomass and increases in plant photosynthesis, the potential of artificial humic acids to assist carbon neutrality was briefly calculated. This work provides a basis for a better understanding of the hydrothermal synthesis of artificial humic acids and the environmental implications of this approach. The findings will shed light on using renewable resources and constructing a closed loop of C in environments.

2 Experimental design

2.1 Artificial humic acids production

Feedstocks were collected locally near Wuxi, Jiangsu, China and ground into powders for hydrothermal humification. The determination method for the contents of lignin, cellulose, and hemicellulose in feedstocks was referred to Zimmer (1999). Moreover, the elemental composition of feedstocks was determined using an elemental analyzer (Unicube, Elementar Analysensysteme GmbH, Germany), with sulfanilamide as the standard substance. Lignin accounted for 5.47%, 19.81%, 10.42% and 4.82% of CL, CS, PS, and MC biomasses, respectively; cellulose was 32.71%, 32.05%, 17.32% and 38.52% of CL, CS, PS, and MC biomasses, respectively; and hemicellulose was 9.38%, 17.86%, 10.48% and 17.09% of CL, CS, PS, and MC biomasses, respectively (Table S1). The C/N was 8.01, 7.67, 10.35, and 5.38 for CL, CS, PS, and MC, respectively (Table S1).

Hydrothermal humification synthesis of artificial humic acids was conducted in a 100 mL autoclave at 200 °C for 48 hours. The ratio of feedstock solid and alkaline solution of KOH (initial pH = 13) was 1:20 (Yang et al. 2021). To investigate the humification process of different kinds of feedstocks, both the undecomposed biomass and the produced solution were dynamically sampled at 0.3, 1, 3, 7, 14, 24, and 48 h, respectively. The liquid samples were separated from undecomposed biomass using qualitative filter membranes (Titan, Shanghai, China) and then filtered with a 0.22 μm polyether sulfone filter (Titan, Shanghai, China) for characterization. Dynamic changes in pH, total organic carbon (TOC) contents, and compositions of the liquid samples during humification processes were determined using a pH analyzer (Mettler-Toledo, Shanghai, China), a Total Organic Carbon analyzer (TOC-VCPH, SSM-5000A, Shimadzu, Japan), and a three-dimensional fluorescence spectrometer (F-320, Agilent Technologies, USA), respectively. The liquid samples collected at 48 h were artificial humic acids products, which were named AHA_{CL}, AHA_{CS}, AHA_{PS}, and AHA_{MC}, representing the artificial humic acids from CL, CS, PS, and MC, respectively.

2.2 Artificial humic acids characterization

The composition of artificial humic acids was determined using a three-dimensional fluorescence spectrometer (F-320, Agilent Technologies, USA) and ultra-performance liquid chromatography-mass spectrometry (UPLC-MS/MS) (Thermo Scientific UPLC Vanquish, Thermo Fisher Scientific). Specifically, the excitation and emission wavelength used for scanning of fluorescence spectroscopy ranged from 200 to 450 nm at 5 nm intervals and from 200 to 550 nm at 2 nm increments, respectively. As for UPLC-MS/MS analysis, the artificial humic acids were centrifugated at 12,000 g for 10 minutes to remove impurities and then dissolved in dimethyl sulfoxide (Adamas Reagent Company, Shanghai). The UPLC conditions were as follows: mobile phase of 0.1% formic acid and 0.1% formic acid acetonitrile solution with a flow rate of 0.35 mL min^{-1}; an ACQUITY UPLC HSS T3 column (2.1 × 100 mm, 1.8 μm) with column temperature maintained at 35 °C during analysis; and electrospray-time of flight mass spectrometry with maximum IT of 100 ms, scanning in a range from 70 to 1050 m z^{-1} and duration of 18 minutes.

The structural property of the artificial humic acids was characterized using an X-ray photoelectron spectroscopy (XPS) (Thermo Fisher Nexsa, Thermo Fisher, USA). The elemental composition including C, N, oxygen (O), and hydrogen (H) in the artificial humic acids

was determined using an elemental analyzer (Unicube, Elementar Analysensysteme GmbH, Germany) with sulfanilamide as standard substances. Contents of nutrients such as phosphorus (P), potassium (K), iron (Fe), magnesium (Mg), sodium (Na), manganese (Mn), sulfur (S), and calcium (Ca) in the artificial humic acids were analyzed using an inductively coupled plasma mass spectrometry (ICP-MS; iCAP-TQ, Thermo Fisher, Germany) equipped with a triple quadrupole.

The redox potential of artificial humic acids was determined using an Oxidation-Reduction Potential (ORP) analyzer (Mettler-Toledo GmbH, Switzerland). Electrochemical analysis of artificial humic acids was conducted in a CHI 660E electrochemical workstation with a three-electrode system (Shanghai Chenhua Instrument Company, China). Specifically, in the cyclic voltammetry experiments, a glassy carbon electrode, a platinum wire, and a saturated Ag/AgCl (+0.197 V vs. standard hydrogen electrode) served as the working, counter, and reference electrodes, respectively. All tests were conducted in 27 ml of 0.1 M KCl solution (pH = 7). The working electrode was poised at +0.42 and −0.68 V. After the background currents stabilized, 3 mL of artificial humic acids were spiked to the reactor, and the electron transfer capacity (ETC, μmol e^- [ml C]$^{-1}$) of artificial humic acids was calculated by eq. (1).

$$\mathrm{ETC} = \mathrm{Ap}/\left(e^{*}V^{*}N_A\right) \quad (1)$$

where Ap (coulomb, C) is the integral based on cyclic voltammetric curves, N_A is the Avogadro's constant with $6.02\times10^{23}\,\mathrm{mol}^{-1}$ in default, e is the amount of electrical charge per unit 1.6×10^{-19} C, V (mL) is the volume of artificial humic acids.

2.3 Hydroponic study in a greenhouse

To investigate the potential and mechanisms of artificial humic acids to promote plant photosynthesis, a hydroponic study of corn (Shiyu No. 9) was conducted in a greenhouse. This avoided the influence of soil properties on plant growth, and we will test the interaction between different artificial humic acids and soils in our following studies. The corn seeds were purchased from Qingdao seed station, Qingdao, China. The seeds were sterilized with 10% H_2O_2 for 10 minutes and then rinsed with deionized water repeatedly before incubation. Seeds were first placed at 25 °C in dark for 3 days for germination, and then uniform corn seeding was selected and incubated in 2.5 dm^3 ceramic jars with 1/4 Hoagland nutrient solution (mmol L^{-1}): $Ca(NO_3)_2{\cdot}4H_2O$, 1.0; KNO_3, 0.25; $NH_4H_2PO_4$, 0.25; $MgSO_4{\cdot}7H_2O$, 0.5; $MnSO_4{\cdot}H_2O$, 2.39×10^{-3}; H_3BO_3, 0.012; $ZnSO_4{\cdot}7H_2O$, 1.91×10^{-4}; $CuSO_4{\cdot}5H_2O$, 0.8×10^{-4}; $(NH_4)_6Mo_7O_{24}$, 0.41×10^{-6}; Fe-EDTA, 0.01. Artificial humic acids were applied into the nutrient solution at the three leaves and one core stage of corn (for 14 days after seed sowing). It was reported that the photosynthesis of corn in this stage is commonly the most vigorous, being sensitive to the application of fertilizer (Liu et al. 2020). The application volume of artificial humic acids in 2 L of nutrient solution is 40 mL, and the final nutrient concentration of the solution is equal to that of 1/4 Hoagland nutrient solution (Table S2). A control treatment with only Hoagland nutrient solution was conducted at the same time. The five treatments are named P_{CK} (no artificial humic acids), P_{CL} (applied with AHA_{CL}), P_{CS} (applied with AHA_{CS}), P_{PS} (applied with AHA_{PS}), and P_{MC} (applied with AHA_{MC}), and each treatment was performed in six replicates. All ceramic jars were placed in a greenhouse with natural light and a day and a night temperature of 25–30 and 15–18 °C, respectively.

Parameters associated with plant photosynthesis were determined after 7 days of application of artificial humic acids. Specifically, the relative content of Chlorophyll in the second top leaf of each plant was measured by Chlorophyll Meter (SPAD-502 plus, Konica Minolta Inc., Japan) to represent the chlorophyll content of the whole plant. During measurement, the ambient CO_2 concentration, relative humidity, maximum photosynthetic photon flux density, and leaf temperature were 400 μmol mol^{-1}, 60%, 500 μmol $m^{-2}s^{-1}$, and 25 °C, respectively. During photosynthesis, the fluorescence intensity of the chlorophyll rises from an initial minimum fluorescence intensity (Fo) to maximal fluorescence intensity (Fm) during 1 s of illumination with saturating red light (Liu et al. 2020). Fluorescence parameters including Fo and Fm of the chlorophyll were measured using a chlorophyll fluorescence imaging system (Pocket PEA, Hansatech Instruments Ltd., UK). The maximum photochemical efficiency (φ[Po]) of the PSII process was calculated by Fv/Fm, where Fv is the difference between Fm and Fo (Niu and Croue 2019). Moreover, fluorescence parameters involved in light energy absorption, energy transfer, conservation, thermal dissipation, and PSII photoactivity were also determined using a plant efficiency analyzer (Pocket PEA, Hansatech Instruments Ltd., UK). The description of fluorescence parameters is shown in Table S3. The net photosynthetic rate (Pn) of each plant was determined using a CIRAS-3 portable gas exchange system (CIRAS-3, PP-Systems, USA). After the determination of plant photosynthesis, the plants were collected for biomass and length analysis. The content of C and N in corn leaves was determined by the elemental analyzer (Unicube, Elementar Analysensysteme GmbH, Germany).

2.4 Potential of artificial humic acids on carbon neutrality

The potentials of artificial humic acids serving for carbon neutrality were calculated. Conversion of biomass into artificial humic acids mainly avoids C loss during natural decomposition and human activities. The CO_2 emission in hydrothermal humification processes is negligible, which also supports the green synthesis of the artificial humic acid approach (Manasrah et al. 2020). C reuse rate (Cr) of feedstocks is calculated by eq. (2); promotion of photosynthetic C fixation by artificial humic acids (Pr) is calculated by eq. (3); promotion of plant biomass C by artificial humic acids (CPr) is calculated by eq. (4). Data on the global average atmospheric C pool, terrestrial vegetation C pool, and photosynthetic C sequestration are referred to (Yang and Antonietti 2020a; Tables S4 and S5).

$$\mathrm{Cr}(\%) = \left[\frac{\left(C_{AHA} * \frac{V_{AHA}}{1000}\right)}{C_F * 3}\right] * 100 \quad (2)$$

$$\mathrm{Pr}\,(\%) = \left[\frac{(A_{AHA} - A_{CK})}{A_{CK}}\right] * 100 \quad (3)$$

$$\mathrm{CPr}(\%) = \left[\frac{C_{AHA} * B_{AHA} - C_{CK} * B_{CK}}{C_{CK} * B_{CK}}\right] * 10 \quad (4)$$

where C_{AHA} ($g\,L^{-1}$) is the content of total organic C in artificial humic acids; V_{AHA} (mL) is the volume of artificial humic acids; C_F (%) is the content of C in feedstocks determined by element analysis; and the weight of feedstocks used in the hydrothermal humification process is 3 (g); A and A_{CK} (μmol CO_2 $m^{-2}s^{-1}$) are the net photosynthetic rate of corn in the treatments with artificial humic acids applied and in the P_{CK}, respectively; C_{AHA} and C_{CK} (%) are the content of C in corn in the treatments with artificial humic acids applied and in the P_{CK}, respectively; B_{AHA} and B_{CK} (g) are the content of fresh biomass of the corn in the treatments with artificial humic acids applied and in the P_{CK}, respectively.

2.5 Statistical analysis

Statistical analysis of the data was performed using IBM SPSS Statistics (SPSS v.23.0, IBM, Armonk, NY, USA) by a one-way ANOVA with Tukey HSD post hoc test after verification of normality and homoscedasticity assumptions, and the a *p*-value of less than 0.05 was considered statistically significant. The excitation-emission matrices (EEMs) based on the results of the three-dimensional fluorescence spectrum were decomposed by Parallel Factor Analysis (PARAFAC) using the DOMFluor toolkit in MATLAB (R2021b) (Henderson et al. 2009). The characteristic substances of artificial humic acids derived from different feedstocks were selected by Venn analysis (http://www.ehbio.com/test/venn/; Chen et al. 2021). We further performed a pathway enrichment analysis for these characteristic substances to investigate their potential effects on plant metabolism (http://www.metaboanalyst.ca/) (Wang et al. 2022). Principal component analysis and pair-wise correlation analysis were performed in R (v.4.1.2) using the "corrplot", "FactoMineR", "factoextra", and "ggplot2" packages. Correlation heatmaps were conducted in OriginPro (v.2022b) with the Correlation Plot package. Co-occurrence networks were visualized using Cytoscape (v.3.8.2).

3 Results

3.1 Hydrothermal process of different feedstocks

The degradation curves of different feedstocks can be well fitted by the pseudo-second-order kinetic model (Fig. 1A). A fast biomass decomposition occurs at the beginning of the 3-hour of hydrothermal humification process with k in the order of CL > CS > PS = MC. After 48 hours of hydrothermal process, biomass degradation achieves equilibrium, and the final degradation ratio (Dr.) is in the order of MC > PS > CL > CS ($p < 0.05$). Compared to CS and PS, MC shows a better humification process as expressed by a higher humification index (HI) value (Fig. 1C) but a more incomplete self-neutralization process (Fig. 1B). CL shows both poor self-neutralization and humification capacity (Fig. 1A and B), suggesting that CL would not be a good feedstock choice for artificial humic acids production.

The results of PARAFAC indicate that dissolved organic matter in solution during hydrothermal humification can be divided into seven kinds of substances (Figs. 1D and S2). The CL mainly decomposed into HA C-like and FA A-like products in the first 20 minutes, and then dominated by protein products in the AHA_{CL} (Figs. 1D and S3). The transformation pattern of CS and PS during the humification process is similar, showing that the feedstocks are decomposed into FA A-like products, and then transformed into protein products, and finally condensed into artificial humic acids with FA M-like and protein products dominated (Figs. 1D and S3). The fluorescence intensity of the products derived from CS is stronger than that from PS (Fig. 1D), consistent with the results of HI (Fig. 1C). The transformation pattern of MC during the humification process is different from that of CL, PS, and CS. The MC mainly decomposed into FA A-like products in the first 20 minutes, and then transformed into FA M-like products, and finally condensed into AHA_{MC} being dominated by FA M-like, FA A-like, and HA C-like products (Figs. 1D and S3).

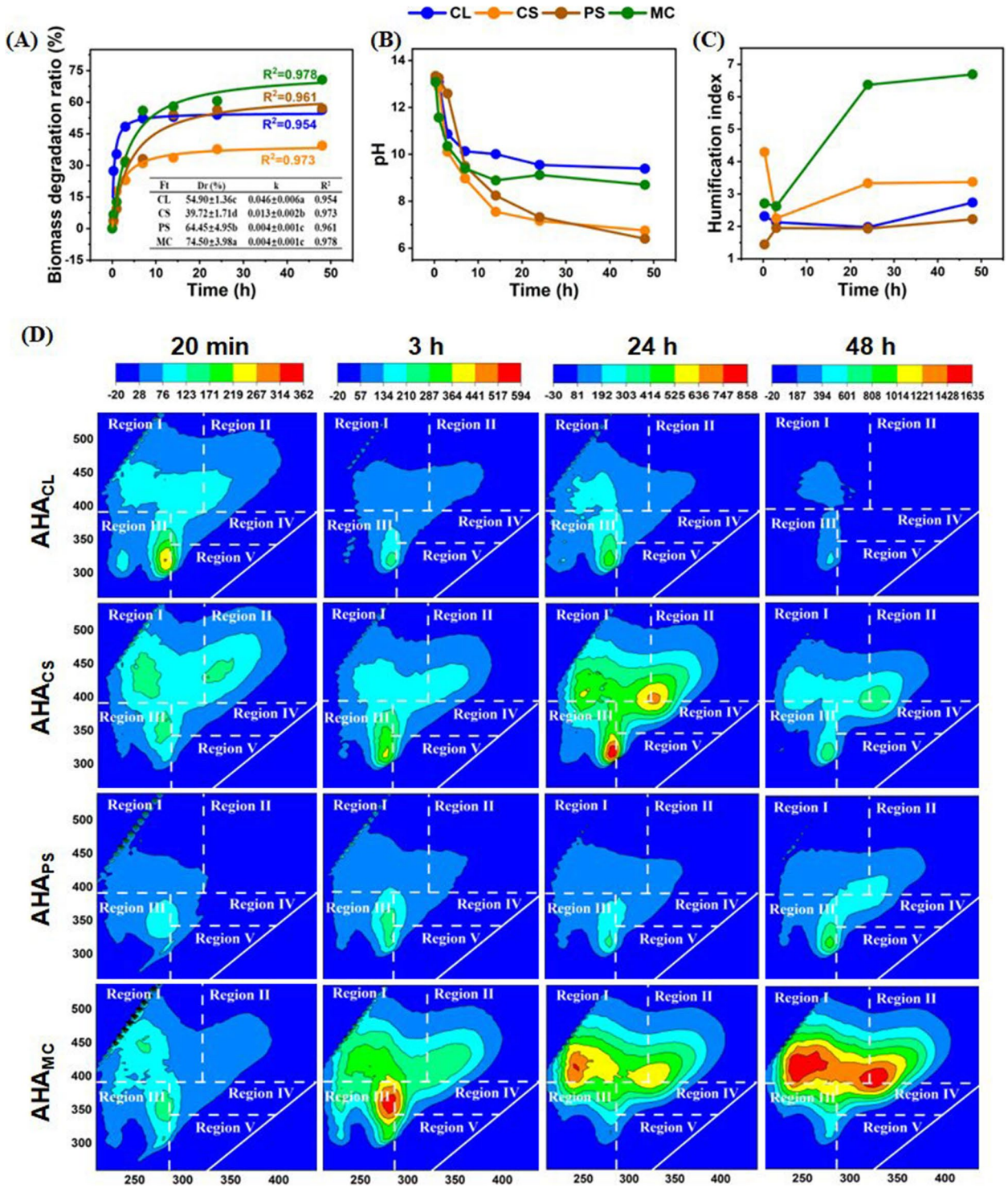

Fig. 1 Changes in (**a**) biomass degradation rate, (**b**) pH, (**c**) humification index (HI) and (**d**) excitation-emission matrix (EEMs) of solutions during the hydrothermal humification process of different feedstocks. CL, CS, PS, and MC are the abbreviations of camphor leaves, corn stalks, peanut shells, and mixed cyanobacteria, respectively. The lines in Fig. 1A represent the fitting curves based on a pseudo-second-order kinetic model, where Ft means feedstock type, Dr. is the degradation ratio of biomass and k is the degradation rate during the humification process. The classification of decomposed substances in artificial humic acids in Fig. 1D is based on the results from parallel factor analysis in Fig. S2

3.2 Properties of different artificial humic acids

Three typical characteristic peaks including C1s, O1s and N1s were observed at 531.7, 399.2 and 532.6 eV, respectively, in the XPS spectrum (Fig. S4A). The high-resolution C1s spectra were commonly fitted by four peaks corresponding to C=O at 285.5 eV, C-O at 284.9 eV, C-N at 284.2 eV and C-C at 283.7 eV in the artificial humic acids (Fig. 2A). In addition, the O=C-O at 287.9 eV exists in AHA_{CS}, AHA_{PS}, and AHA_{MC}; the C-Cl at 287.3 eV exists in AHA_{PS} and AHA_{MC}; the COOR at 288.4 eV specifically exists in AHA_{PS}. The high-resolution O1s spectra were commonly fitted by C-O at 531.2 eV and C=O at 530.4 eV in the artificial humic acids (Fig. 2A). Moreover, there were R-OH at 531.8 eV and O=C-O at 532.5 eV

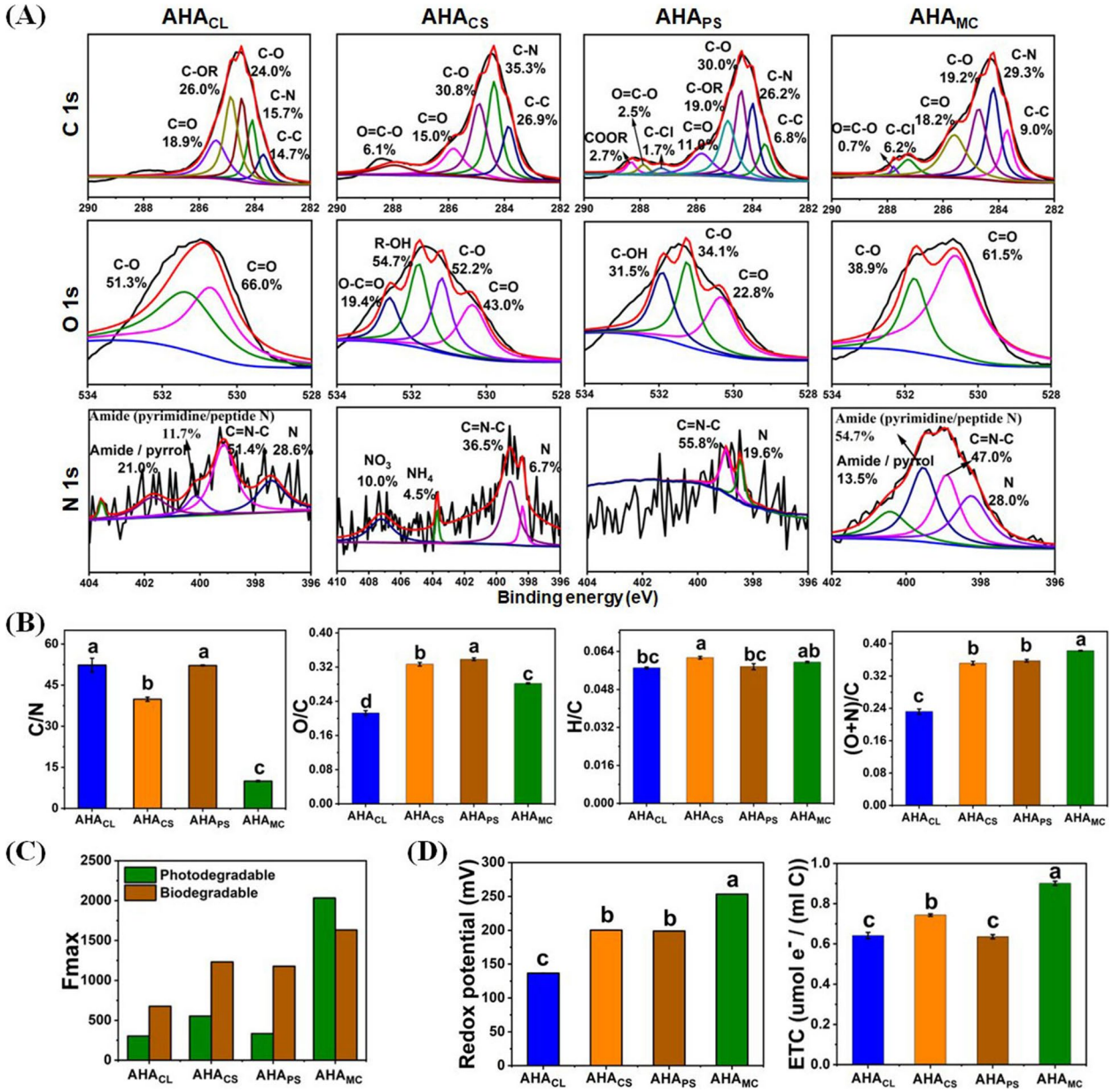

Fig. 2 The properties of different artificial humic acids. **a** X-ray photoelectron spectroscopy high-resolution scan of the C1s, O1s, and N1s signals; **b** the property of carbon structure as reflected by the ratio of other elements and carbon; **c** contents of photodegradable and biodegradable substance in artificial humic acids; **d** redox potential and electron transfer capacity (ETC) of different artificial humic acids; in Fig. 3C, the photodegradable substances include FA A-like, HA C-like, and HA A-like humic acids, and the biodegradable substances include protein-like, tyrosine-like, FA A-like, and HA A-like humic acids (Mostofa et al. 2013). Bars in Fig. 2B and D represent the standard error values ($n = 3$). Different letters above each column denote statistical significance among treatments at $p < 0.05$ level (ANOVA, Tukey's HSD)

in AHA_{CS}, which accounted for 54.7% and 19.4% of the O peak area, respectively; there were C-OH at 531.9 eV in AHA_{PS}, which accounted for 31.5% of the O peak area. There were high levels of N in the MC (Table S1), resulting in abundant N-dropped structures in AHA_{MC} (Fig. 2A). The high-resolution N1s spectra of AHA_{MC} were fitted by four peaks corresponding to Amide/pyrrol at 401.8 eV, Amide (pyrimidine/peptide N) at 400.2 eV, C=N–C at 399.3 eV, and N at 398.2 eV (Fig. 2A).

Compared to AHA_{MC}, the C/N values of AHA_{CL}, AHA_{CS} and AHA_{PS} were significantly higher (Fig. 2B). The H/C of artificial humic acids derived from different raw materials did not vary significantly (Fig. 2B). The (O + N)/C and O/C ratios are the lowest in AHA_{CL}, implying a high aromaticity, being consistent with the XPS analysis results. Moreover, similar to natural humic acids, the O/C ratio of all the produced artificial humic acids were less than 0.4 (Fig. 2B).

The AHA_{MC} contains high contents of both photodegradable and biodegradable substances (Fig. 2C), consistent with its high HI value (Fig. 1C) and fluorescence intensity (Fig. 1D). Moreover, there are higher relative contents of photodegradable substances than biodegradable substances in AHA_{MC}, which is contrary to the substance compositions in AHA_{CL}, AHA_{CS} and AHA_{PS} (Fig. 2C). AHA_{CL} contains the highest nutrients content (Fig. S5). Compared to other kinds of artificial humic acids, AHA_{MC} contains more S (Fig. S5).

The cyclic voltammetry curves of artificial humic acids showed redox peaks without typical rectangular features (Fig. S4B). In particular, the redox potential and the ETC value were the highest in AHA_{MC} and the lowest in AHA_{CL} (Fig. 2D).

3.3 Promotion mechanisms of different artificial humic acids on corn photosynthesis

The application of artificial humic acids benefits corn growth (Fig. S6). The contents of C in corn leaves but not the corn biomass were significantly increased by artificial humic acids (Figs. S7 and S8). Therefore, artificial humic acids probably promoted the C fixation of plants' photosynthesis. Compared to the P_{CK} treatment, the net photosynthetic rate of corn increased by 69.17%, 113.17%, 69.17%, and 117.84% in the P_{CL}, P_{CS}, P_{PS}, and P_{MC} treatments, respectively (Fig. 3B). The AHA_{MC} also significantly increased the chlorophyll content (SPAD) in corn leaves by 37.89% (Fig. 3A).

In light reaction system, the application of artificial humic acids did not improve the state of the photosynthetic apparatus as expressed by PI_{abs} in corn (Fig. 3C and Table S3). The quantum yields for electron transport (φ[Eo]) and thermal energy dissipation (φ[Do]) were also not improved by artificial humic acids (Fig. 3E). The captured light energy had been consumed for reduction of primary plastoquinone electron acceptor in the PSII process (ETo/RC) and electron transport in the reaction center (TRo/RC), accompanied by an increased thermal energy dissipation (DIo/RC) (Fig. 3G). However, the application of artificial humic acids significantly increased the reduction rate of primary plastoquinone electron acceptor in PSII (Mo) but not the volume of the plastoquinone pool for PSII reaction (Sm) (Fig. 3F). Moreover, AHA_{MC} specifically improved the φ(Po), the efficiency of electron transfer (ψo), and the number of electrons for the reduction of primary plastoquinone electron acceptor in PSII (N) (Fig. 3D and F), which further contributed to the increased light energy absorption as expressed by ABS/RC in corn leaves (Fig. 3G).

In dark reaction system, the synthesis of ATP and NADPH can be assisted by protons from the cleavage of water, while decreased by the CO_2 absorption and conversion. AHA_{CL} and AHA_{CS} improved the transpiration rate (E) and stomatal conductance (Gs) but decreased intercellular CO_2 concentration (Ci) and ATP contents in corn leaves in P_{CL} and P_{CS} treatments. AHA_{PS} promoted transpiration rate and stomatal conductance of corn leaves and inhibited CO_2 conversion, resulting in increased ATP contents in corn leaves in P_{PS} treatment (Fig. 3G).

The application of artificial humic acids not only changes photochemical parameters in corn leaves, but also participates in plant metabolism. The compositions of artificial humic acids are dependent on the lignocellulose content in feedstocks (Fig. S9A and B). All the four kinds of artificial humic acids have the potential to stimulate phenylalanine metabolism in plants since they contain photosynthetic components (Fig. S9C). Specifically, the AHA_{CL}, AHA_{CS} and AHA_{PS} can also participate in pyruvate metabolism and AHA_{MC} can participate in glyoxylate and dicarboxylate metabolism in plants (Fig. S9C).

3.4 Effects of feedstock properties on humification process and corn photosynthesis

During the humification process, both the Dr. and k of feedstocks were negatively correlated with the content of lignin (Fig. 4A; $p < 0.05$). Compared to MC feedstocks, CS, a kind of typical carbon-rich and lignocellulose-abundant biomass (Table S1), is not conducive to the hydrothermal humification process. The low C/N, high H/C, and high cellulose contents in feedstocks are favorable to their hydrothermal humification (Fig. 4A).

The relative abundance of lignin, cellulose and hemicellulose, and the C/N and H/C ratios of feedstocks are the main drivers for the compound compositions and properties of artificial humic acids (Fig. 4B). Specifically,

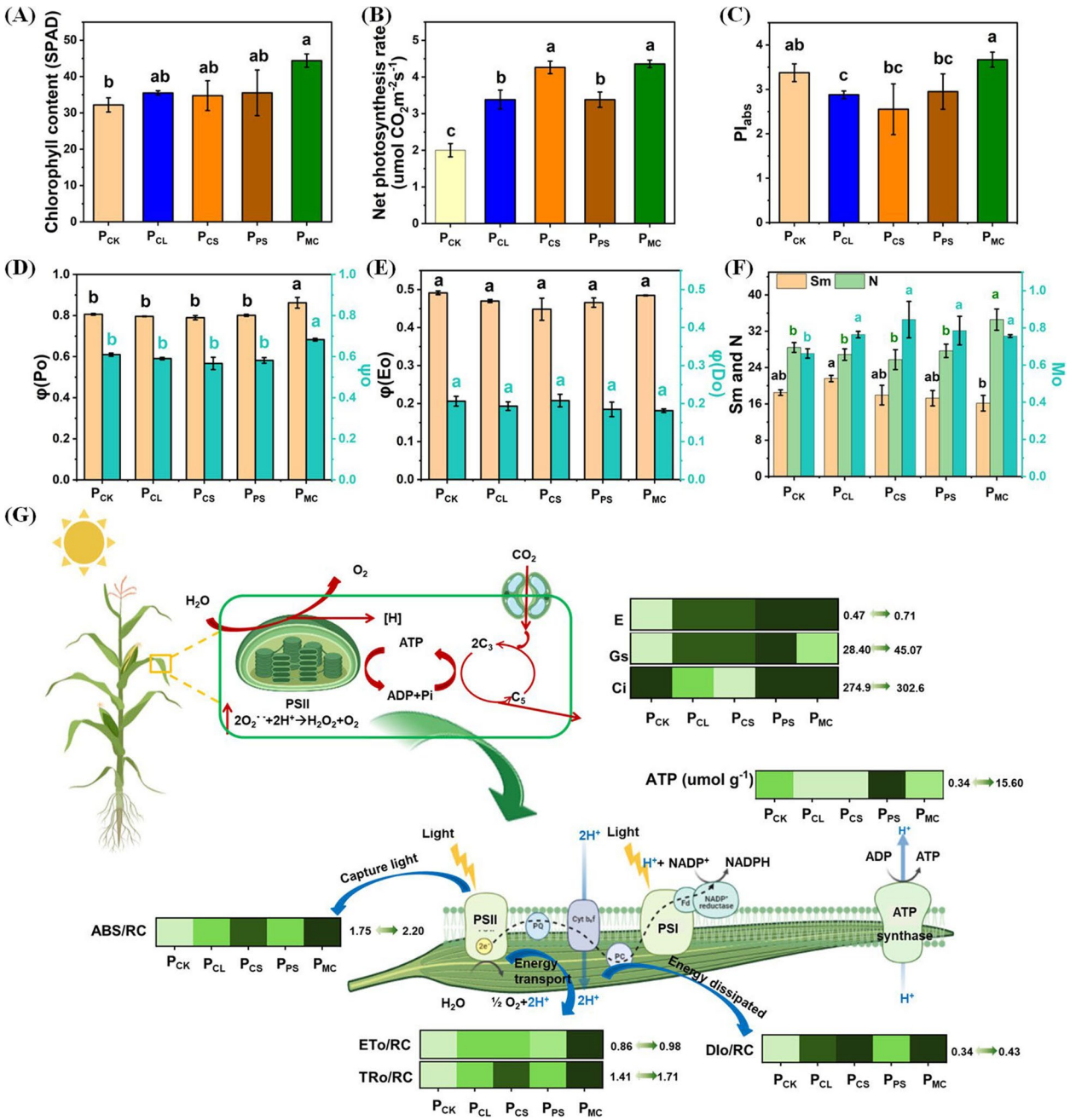

Fig. 3 Effects of artificial humic acids on corn photosynthesis. **a** Contents of chlorophyll; **b** net photosynthetic rate; **c** performance index (PI_{abs}) of the photosynthetic apparatus; **d** maximum photochemical efficiency (φ[Po]) and efficiency of electron transfer beyond the reduction of primary plastoquinone electron acceptor of PSII (ψo); **e** quantum yield for electron transport (φ[Eo]) and thermal energy dissipation (φ[Do]); **f** the number of electron for reduction of primary plastoquinone electron acceptor of PSII (N), the volume of plastoquinone pool (Sm) and the rate of reduction of primary plastoquinone electron acceptor of PSII (Mo); **g** schematic diagram of a photosynthetic process as affected by artificial humic acids. Bars in Fig. 3A-F represent the standard error values ($n = 3$). Different letters above each column denote statistical significance among treatments at $p < 0.05$ level (ANOVA, Tukey's HSD). In Fig. 3G, E, Gs, and Ci represent the transpiration rate, stomatal conductance, and intercellular CO_2 concentration during photosynthesis of corn leaves, respectively. ABS/RC, TRo/RC, ETo/RC, and Dlo/RC indicate the absorption, capture, transformation, and dissipation of light energy per unit reactive centers of plant leaves during PSII process, respectively

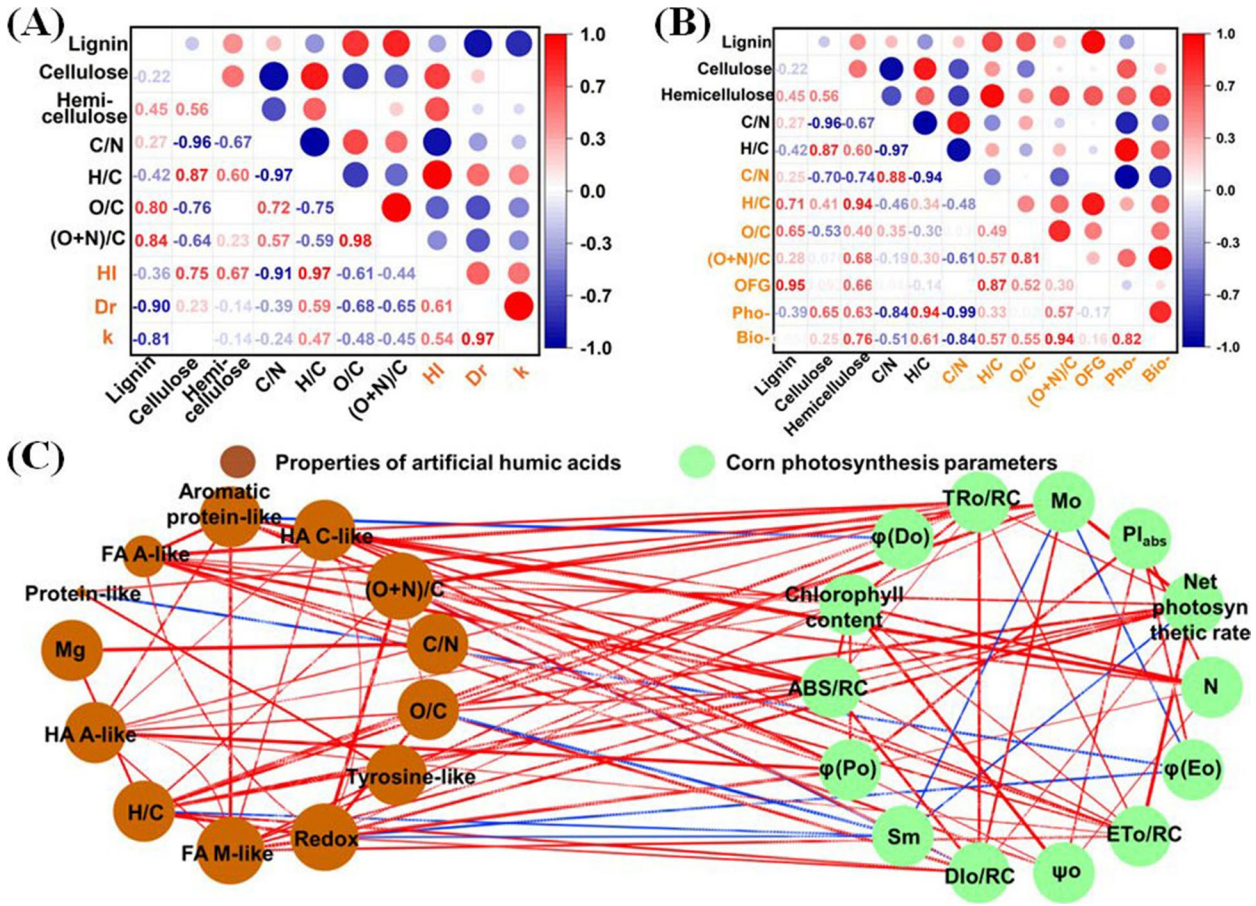

Fig. 4 Dependence of (**a**) the humification process and (**b**) the properties of artificial humic acids on feedstock properties, and (**c**) a co-occurrence network of the properties of artificial humic acids and corn photosynthesis parameters. In Fig. 4A, HI is the humification index, Dr. is the degradation ratio of biomass and k is the degradation rate during the humification process. The Pho-, Bio-, and ETC in Fig. 4B are the abbreviations of photodegradable substances, biodegradable substances, and electron transfer capacity, respectively. In Fig. 4A and B, the properties of feedstocks are in black font and that of humification process and artificial humic acids are both in orange font. The red and blue lines in the co-occurrence network represent a significant positive and negative relationship between parameters, respectively; only the lines with correlation rate (r) > 0.8 was illustrated in this network (Gao et al. 2022); the node size of each parameter is in line with the correlation relationship numbers between each parameter

high contents of hemicellulose in feedstocks such as MC contribute to high H/C, O/C and (O + N)/C ratios but low C/N ratio of artificial humic acids (Fig. 4B). In addition, the photodegradable substances of artificial humic acids are mainly produced from the feedstocks with a high relative abundance of cellulose and hemicellulose, a high H/C ratio but a low C/N ratio. While, the biodegradable substances are mainly produced from the feedstocks with a high relative abundance of hemicellulose. The redox and the ETC of artificial humic acids were significantly and positively correlated with the content of hemicellulose and the H/C ratio but negatively correlated to the feedstock C/N (Fig. 4B). Therefore, the feedstocks with high H/C and hemicellulose content (e.g., MC) are prone to produce artificial humic acids with abundant photodegradable and biodegradable substances and a strong ability for electron transfer. They should be kinds of high-quality feedstocks for the production of artificial humic acids.

The structures and compound compositions of artificial humic acids determine their properties and functions (Figs. 2A and S5). Increases in Pn and ABS/RC of corn benefited from the FA/HA A-like and HA C-like fluorescent substances in artificial humic acids (Fig. 4C). HA A-like fluorescent substances, another kind of photodegradable component in artificial humic acids, mainly promoted the photochemical efficiency of leaves (ϕ[Po]). The contents of aromatic protein-like, Tyrosine-like and FA M-like substances in artificial humic acids contributed to the improved net photosynthetic rate and

chlorophyll content in leaves. While, the aromatic protein-like and protein-like substances in artificial humic acids were significantly and negatively correlated with the thermal energy dissipation (ϕ[Do]) and the quantum yields for electron transport (ϕ[Eo]), respectively. As for structural properties of artificial humic acids, their H/C and O/C ratios positively correlated with the net photosynthetic rate of plants while negatively correlated with the volume of plastoquinone pool in PSII (Sm) ($p < 0.05$); their H/C and (O + N)/C ratios significantly positively correlated with the reduction rate of primary plastoquinone electron acceptor of PSII (Mo) ($p < 0.05$), and their C/N ratio was positively correlated with the light energy for reduction rate of primary plastoquinone electron acceptor and transport of PSII as expressed by TRo/RC and ETo/RC; the (O + N)/C ratio in artificial humic acids was also negatively correlated with the volume of plastoquinone pool in PSII (Sm) ($p < 0.05$). The ETC and redox potential of artificial humic acids were positively correlated with the net photosynthetic rate ($p < 0.05$), the light energy for reduction rate of primary plastoquinone electron acceptor and transport of PSII as expressed by TRo/RC and ETo/RC of plants. It is well known that the absorption of light energy by chlorophyll initiates the light reaction in photosynthesis. The promotion mechanisms of artificial humic acids for plant photosynthesis could be attributed to the promotion of light energy capture and transfer.

4 Discussion

4.1 Properties of artificial humic acids and the mechanisms that promote photosynthesis are feedstock-dependent

The hydrothermal humification process is similar to the traditional humification of biomasses (Byun et al. 2021). The feedstocks with low C/N such as MC can be cracked into monomers containing functional groups such as amino, which is easy to be condensed, resulting in a high HI in the artificial humic acids (Jiménez-González et al. 2020). In addition, lignin contains abundant fused-ring structure and high-energy bonds, making it highly resistant to decomposition (Ma et al. 2018; Ralph et al. 2019). Straw usually has high carbon recycling potential and it is a main agricultural renewable resource for biochar and compost production (Yang and Antonietti 2020b). However, compared to CS feedstocks, MC is a better choice for hydrothermal humification process. Moreover, the AHA_{MC} contains less O=C-O and C-O but abundant N-dropped structures (Fig. 2A), resulting in a poor aromatization (Jiménez-González et al. 2020). Low O/C ratio in AHA_{MC} is an indicative of abundant carboxylic acids or furans structures existing in the humic acids (Yang et al. 2021), being conducive to the formation of photodegradable substances and thus benefiting redox reactions during plant photosynthesis. The diverse N-dropped structures such as amide (pyrimidine and peptide N) and C=N-C in AHA_{MC} also contribute to their high redox potential and ETC (Jiménez-González et al. 2020). This kind of artificial humic acids produces many electrons and free radicals to favor electron transfer during a redox process (Chen et al. 2016).

The increased photosynthesis by AHA_{MC} can be partly ascribed to the increased light energy capture for the reduction of primary plastoquinone electron acceptor and transport in PSII process (Fig. 3). Other exogenous materials such as La_2O_3 nanoparticles can also improve plant photosynthesis with the similar mechanisms (Liu et al. 2020). In addition, another humic substance, fulvic acids, accelerated the absorption rate of photons in thylakoids to promote photosynthesis of chrysanthemums (Fan et al. 2014). Moreover, there are abundant nutrients including N, P, K, Mg, S, Fe, Na, Ca, and Mn in artificial humic acids (Figs. S4 and S6). It is well known that N and Mg play important roles in the synthesis of chlorophyll in plant leaves (Liu et al. 2020). Sufficient N supply benefits CO_2 diffusion (Ci) and the biochemical cycle of nutrients in leaves, resulting in strong plant photosynthesis (Huang et al. 2022). K is an activator of various enzymes that participate in plant photosynthesis (Swift et al. 2021). Therefore, nutrients supply is another mechanism by which AHA_{MC} promotes corn photosynthesis mostly (Fig. 3).

With the application of artificial materials (e.g., Fe-based nanoparticles), many energy-consuming pathways including photorespiration, alanine metabolism and branch chain amino acid biosynthesis had been shut down, benefiting plant photosynthesis (Li et al. 2018; Li et al. 2020). Artificial humic acids can also induce metabolism in corn leaves and thereby favouring nutrient uptake and plant photosynthesis (Li et al. 2020). AHA_{MC} specifically affects glyoxylate and dicarboxylate metabolism that related to plant C metabolism and photosynthesis (Ma et al. 2018), which can be ascribed to more photodegradable substances and higher redox potential in AHA_{MC} (Fig. 2C and D). Moreover, the aliphatic and carboxyl structures in artificial humic acids promote the synthesis of nutrients and increase the associated enzyme activity in leaves, respectively, both of which benefit plant photosynthesis (Byun et al. 2021).

Artificial humic acids produced from the hydrothermal humification of waste biomasses show great potential in photosynthesis promotion. In this case, the artificial humic acids derived from feedstocks with high H/C and low content of lignin and C/N can improve light energy capture and light energy conversion efficiency in the PSII process, increasing plant photosynthesis. In contrast, higher content of lignin and C/N in feedstocks can

produce artificial humic acids that increase plant photosynthesis by providing functional enzymes (proteins) and nutrients for leaves. Currently, CO_2 fixation during plant photosynthesis contributes less C sequestration in environments (Yang and Antonietti 2020a). Improving the C fixation ability of plants is crucial for promoting C neutrality from the viewpoint of global concern. It is important to fully understand the promotion mechanisms of artificial humic acids on plant photosynthesis for their precise and worldwide application.

4.2 Artificial humic acids show great potential for carbon neutrality

Take China as an example, there was about 3.49 Gt of discarded biomass C from forests and croplands in 2020, which will reach 3.80 Gt by 2030 (https://www.beipa.org.cn/); specifically, the annual biomass yields of CL, CS and PS are 0.40, 0.81 and 0.05 Gt, respectively (Table S7), and the annual algae production in Taihu Lake in China was about $6.8*10^{-3}$ Gt in 2018 (http://www.tba.gov.cn/) resulted from the eutrophication of water. However, less than 3% of the CS and 0.1% of PS or MC have been recycled (Zhi et al. 2022). The accumulation of a large amount of waste biomass causes environmental pollution (McDonough 2016). It was reported that 46% of biomass C was lost into the atmosphere (Zhang et al. 2022), leading to climate warming from CO_2 emissions. To achieve the ecological goal of C emission peaking and neutrality, how to efficiently recycle waste biomasses has been a big concern in the world. However, the development of relevant technologies is still in its infancy (Fig. S10).

Producing artificial humic acids from waste biomass renders C to enter a closed-loop internal cycle of C rather than ending its life (Fig. 5). In the closed-loop C cycle, waste biomass C is transformed into active C in artificial humic acids through an environmentally friendly hydrothermal humification approach (Yang et al. 2021). On one hand, this approach prevents CO_2 emissions during the natural decomposition of biomasses. On the other hand, based on this study, about 8% of biomass C (C_r) can be converted to active organic C in artificial humic acids during the hydrothermal humification of waste biomasses (Table S6). Biomass C will be recycled during the preparation and the environmental application of artificial humic acids and finally be sequestrated in soils (Fig. 5). With the application of artificial humic acids, the contents of available nutrients and microbial activities in soils can be improved (Yang et al. 2021). The improved soil quality enables the promotion of soil C sequestration (Fig. 5) and plant growth (Figs. S6 and S7). Improvements on soil organic matter are promising in curing the climate crisis in a large range of area (Yang and Antonietti 2020a, 2020b). It was calculated that the CO_2 emissions in the atmosphere can be neutralized by increasing approximately 0.4% of C fixation in soils (Yang et al. 2021).

Due to human activities, the annual CO_2 emissions are more than 400 Gt in the world (McDonough 2016).

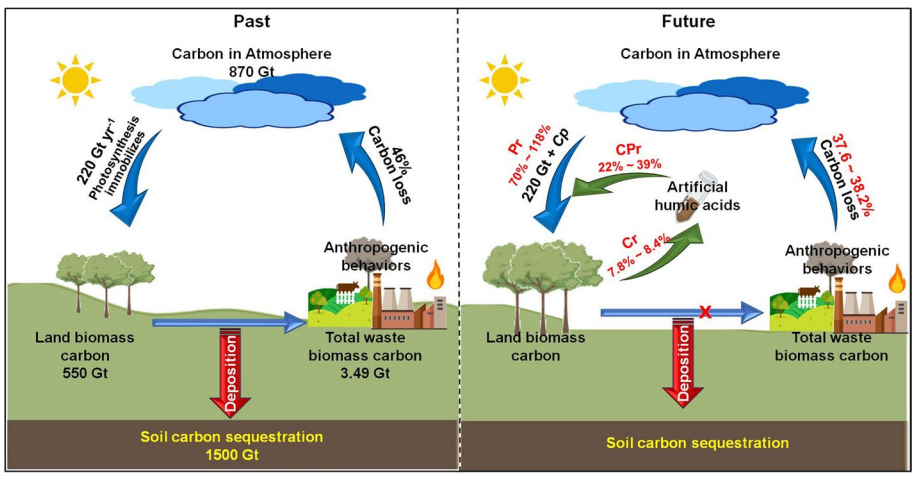

Fig. 5 Diagram of the potential of artificial humic acids application for carbon neutrality. It was reported that the carbon pool in the atmosphere, land biomass, and soil are 870, 550, and 1500 Gt, respectively, and the annual carbon fixation amount during plant photosynthesis is 220 Gt (Yang and Antonietti 2020a). In addition, there are 46% of biomass carbon lost into the atmosphere during its natural decomposition or combustion (Zhang et al. 2020a). The 3.49 and 3.80 Gt represent the discarded biomass carbon in 2020 and 2030, respectively, and the data only includes the amount of waste biomass carbon in forests and croplands (https://www.beipa.org.cn/). The data in the diagram of the Future part are based on the application outcomes of artificial humic acids, where Cr is the carbon reuse rate of the artificial humic acids from waste biomass carbon, Pr and CPr are the promotion of photosynthetic carbon fixation and plant biomass carbon with the help of artificial humic acids, respectively. The data of carbon loss in the diagram of Future part is calculated by (46% - Cr)

Plant photosynthesis is a key to removing CO_2 from the atmosphere and advancing C neutrality in environments. About 220 Gt of C in the atmosphere is fixed by plants during their photosynthesis every year (Yang and Antonietti 2020a). However, the photosynthetic C fixation efficiency of plants is low since the utilization rate of plants to natural light is generally less than 1% (Zhou et al. 2022). To advance the contributions of photosynthetic C fixation to C neutrality, humans are committed to planting more and more trees, resulting in a large occupation and low-value use of land. We suggest that the application of artificial humic acids increased the photosynthetic C fixation rate of corns (Pr) by about 70–118% and the resultant plant biomass C (CPr) by about 22–39% (Fig. 5 and Table S6).

A proper application of artificial humic acid technology is critical since the hydrothermal humification process, the properties of artificial humic acids, and the resultant mechanisms of artificial humic acids for promoting plant photosynthesis are feedstock-dependent (Figs. 3 and 4), and likely to be plant-dependent. Moreover, our previous study suggested that with the help of catalysts such as $FeCl_3$ and nFe_2O_3, the C conversion of feedstocks can be improved by 39% and 14%, respectively (Zhi et al. 2022). Researchers are calling for the optimization of the hydrothermal humification technology for preparing artificial humic acids. The potential of artificial humic acids for C neutrality can be further increased by optimization of preparation technology and precise application.

5 Conclusions

Artificial humic acids show great potential for C neutrality since they can both decrease C emissions from the natural decomposition of waste biomasses and increase C fixation from plant photosynthesis. However, the properties and photosynthetic promotion mechanisms of artificial humic acids are feedstock-dependent. Lower content of lignin and C/N and higher H/C in feedstocks lead to a higher degree of humification and more abundant photodegradable substances in the artificial humic acids. These kinds of feedstocks such as MC are high-quality for artificial humic acids production. The AHA_{MC} can increase plant photosynthesis by improving light energy capture and light energy conversion efficiency in the PSII process. In contrast, the artificial humic acids derived from feedstocks with high content of lignin and C/N (e.g., AHA_{CS} and AHA_{PS}) can also increase plant photosynthesis by providing functional enzymes (proteins) and nutrients for leaves. Research on improving the humification process of these kinds of feedstocks such as CS and PS should be strengthened in future studies.

Supplementary Information

The online version contains supplementary material available at https://doi.org/10.1007/s44246-023-00085-x.

Additional file 1. Supporting information to this article can be found online.

Authors' contributions

All authors contributed to the study conception and design. Material preparation, data collection and analysis were performed by Xiaona Li, Yancai Zhi, Minghao Jia, Xiaowei Wang and Mengna Tao. The first draft of the manuscript was written by Xiaona Li and Yancai Zhi and all authors commented on previous versions of the manuscript. All authors read and approved the final manuscript.

Funding

This work is supported by the National Natural Science Foundation of China (42107244, 41820104009), Jiangsu Natural Science Foundation (BK20210486), and Jiangsu Planned Projects for Postdoctoral Research Funds (2021K445C), Suzhou University of Science and Technology (XTCXSZ2022–12).

Availability of data and materials

The datasets used or analyzed during the current study are available from the corresponding author on reasonable request.

Declarations

Competing interests

Baoshan Xing is an editor and Zhenyu Wang is an editorial board member for Carbon Research and were not involved in the editorial review, or the decision to publish, this article. All authors declare that there are no competing interests.

Author details

[1]Institute of Environmental Processes and Pollution Control, and School of Environment and Ecology, Jiangnan University, Wuxi, Jiangsu 214122, China. [2]Jiangsu Engineering Laboratory for Biomass Energy and Carbon Reduction Technology, Jiangnan University, Wuxi 214122, Jiangsu, China. [3]Jiangsu Collaborative Innovation Center of Technology and Material of Water Treatment, Suzhou University of Science and Technology, Suzhou 215009, Jiangsu, China. [4]Stockbridge School of Agriculture, University of Massachusetts, Amherst, MA 01003, USA.

Received: 23 July 2023 Revised: 14 November 2023 Accepted: 21 December 2023
Published online: 22 January 2024

References

Byun MY, Kim D, Youn UJ, Lee S, Lee H (2021) Improvement of moss photosynthesis by humic acids from Antarctic tundra soil. Plant Physiol Biochem 159:37–42. https://doi.org/10.1016/j.plaphy.2020.12.007

Chen M, Tong H, Liu C, Chen D, Li F, Qiao J (2016) A humic substance analogue AQDS stimulates Geobacter sp. abundance and enhances pentachlorophenol transformation in a paddy soil. Chemosphere 160:141–148. https://doi.org/10.1016/j.chemosphere.2016.06.061

Chen T, Zhang H, Liu Y, Liu YX, Huang L (2021) EVenn: easy to create repeatable and editable Venn diagrams and Venn networks online. J Genet Genomics 48:863–866. https://doi.org/10.1016/j.jgg.2021.07.007

Dargie GC, Lewis SL, Lawson IT, Mitchard ETA, Page SE, Bocko YE, Ifo SA (2017) Age, extent and carbon storage of the Central Congo Basin peatland complex. Nature 542:86–90. https://doi.org/10.1038/nature21048

Fan H, Wang X, Sun X, Li Y, Sun X, Zheng C (2014) Effects of humic acid derived from sediments on growth, photosynthesis and chloroplast ultrastructure in chrysanthemum. Sci Hortic 177:118–123. https://doi.org/10.1016/j.scienta.2014.05.010

Gao C, Xu L, Montoya L, Madera M, Hollingsworth J, Chen L et al (2022) Co-occurrence networks reveal more complexity than community composition in resistance and resilience of microbial communities. Nat Commun 13:3867. https://doi.org/10.1038/s41467-022-31343-y

Henderson RK, Baker A, Murphy KR, Hambly A, Stuetz RM, Khan SJ (2009) Fluorescence as a potential monitoring tool for recycled water systems: a review. Water Res 43:863–881. https://doi.org/10.1016/j.watres.2008.11.027

Huang G, Peng S, Li Y (2022) Variation of photosynthesis during plant evolution and domestication: implications for improving crop photosynthesis. J Exp Bot 73:4886–4896. https://doi.org/10.1093/jxb/erac169

Jiménez-González MA, Almendros G, Waggoner DC, Álvarez AM, Hatcher PG (2020) Assessment of the molecular composition of humic acid as an indicator of soil carbon levels by ultra-high-resolution mass spectrometric analysis. Org Geochem 143:104012. https://doi.org/10.1016/j.orggeochem.2020.104012

Kamimura N, Sakamoto S, Mitsuda N, Masai E, Kajita S (2019) Advances in microbial lignin degradation and its applications. Curr Opin Biotechnol 56:179–186. https://doi.org/10.1016/j.copbio.2018.11.011

Li P, Wang A, Du W, Mao L, Wei Z, Wang S et al (2020) Insight into the interaction between Fe-based nanomaterials and maize (Zea mays) plants at metabolic level. Sci Total Environ 738:139795. https://doi.org/10.1016/j.scitotenv.2020.139795

Li W, Wu S, Zhang H, Zhang X, Zhuang J, Hu C et al (2018) Enhanced biological photosynthetic efficiency using light-harvesting engineering with dual-emissive carbon dots. Adv Funct Mater 28:1804004. https://doi.org/10.1002/adfm.201804004

Liu Y, Yue L, Wang C, Zhu X, Wang Z, Xing B (2020) Photosynthetic response mechanisms in typical C3 and C4 plants upon La_2O_3 nanoparticle exposure. Environ Sci: Nano 7:81–92. https://doi.org/10.1039/c9en00992b

Ma H, Guo Y, Qin Y, Li YY (2018) Nutrient recovery technologies integrated with energy recovery by waste biomass anaerobic digestion. Bioresour Technol 269:520–531. https://doi.org/10.1016/j.biortech.2018.08.114

Manasrah AD, Vitale G, Nassar NN (2020) Catalytic oxy-cracking of petroleum coke on copper silicate for production of humic acids. Appl Catal B-Environ 264:118472. https://doi.org/10.1016/j.apcatb.2019.118472

McDonough W (2016) Carbon is not the enemy. Nature 539:349–351. https://doi.org/10.1038/539349a

Mostofa KMG, Liu C, Yoshioka T, Vione D, Zhang Y, Sakugawa H (2013) Fluorescent dissolved organic matter in natural waters. In: Mostofa KMG, Yoshioka T, Mottaleb A, Vione D (eds) Photobiogeochemistry of organic matter: principles and practices in water environments. Springer, Berlin Heidelberg, Berlin, Heidelberg, pp 429–559

Niu XZ, Croue JP (2019) Photochemical production of hydroxyl radical from algal organic matter. Water Res 161:11–16. https://doi.org/10.1016/j.watres.2019.05.089

Ralph J, Lapierre C, Boerjan W (2019) Lignin structure and its engineering. Curr Opin Biotechnol 56:240–249. https://doi.org/10.1016/j.copbio.2019.02.019

Shen F, Smith RL Jr, Li J, Guo H, Zhang X, Qi X (2021) Critical assessment of reaction pathways for conversion of agricultural waste biomass into formic acid. Green Chem 23:1536–1561. https://doi.org/10.1039/d0gc04263c

Swift TA, Fagan D, Benito-Alifonso D, Hill SA, Yallop ML, Oliver TAA et al (2021) Photosynthesis and crop productivity are enhanced by glucose-functionalised carbon dots. New Phytol 229:783–790. https://doi.org/10.1111/nph.16886

Vardon DR, Franden MA, Johnson CW, Karp EM, Guarnieri MT, Linger JG et al (2015) Adipic acid production from lignin. Energy Environ Sci 8:617–628. https://doi.org/10.1039/c4ee03230f

Wang Z, Tang J, Zhu L, Feng Y, Yue L, Wang C et al (2022) Nanomaterial-induced modulation of hormonal pathways enhances plant cell growth. Environ Sci: Nano 9:1578–1590. https://doi.org/10.1039/d2en00251e

Wu J, Zhao Y, Wang F, Zhao X, Dang Q, Tong T et al (2020) Identifying the action ways of function materials in catalyzing organic waste transformation into humus during chicken manure composting. Bioresour Technol 303:122927. https://doi.org/10.1016/j.biortech.2020.122927

Yang F, Antonietti M (2020a) Artificial humic acids: sustainable materials against climate change. Adv Sci (Weinh) 7:1902992. https://doi.org/10.1002/advs.201902992

Yang F, Antonietti M (2020b) The sleeping giant: a polymer view on humic matter in synthesis and applications. Prog Polym Sci 100:101182. https://doi.org/10.1016/j.progpolymsci.2019.101182

Yang F, Tang C, Antonietti M (2021) Natural and artificial humic substances to manage minerals, ions, water, and soil microorganisms. Chem Soc Rev 50(10):6221–6239. https://doi.org/10.1039/d0cs01363c

Yang F, Zhang S, Cheng K, Antonietti M (2019) A hydrothermal process to turn waste biomass into artificial fulvic and humic acids for soil remediation. Sci Total Environ 686:1140–1151. https://doi.org/10.1016/j.scitotenv.2019.06.045

Zhang S, Wei Z, Zhao M, Chen X, Wu J, Kang K et al (2020) Influence of malonic acid and manganese dioxide on humic substance formation and inhibition of CO_2 release during composting. Bioresour Technol 318:124075. https://doi.org/10.1016/j.biortech.2020.124075

Zhang Z, Hu G, Mu X, Kong L (2022) From low carbon to carbon neutrality: a bibliometric analysis of the status, evolution and development trend. J Environ Manag 322:116087. https://doi.org/10.1016/j.jenvman.2022.116087

Zhi Y, Li X, Lian F, Wang C, White JC, Wang Z et al (2022) Nanoscale iron trioxide catalyzes the synthesis of auxins analogs in artificial humic acids to enhance rice growth. Sci Total Environ:157536. https://doi.org/10.1016/j.scitotenv.2022.157536

Zhou X, Zeng Y, Lv F, Bai H, Wang S (2022) Organic semiconductor-organism interfaces for augmenting natural and artificial photosynthesis. Acc Chem Res 55:156–170. https://doi.org/10.1021/acs.accounts.1c00580

Zimmer M (1999) Combined methods for the determination of lignin and cellulose in leaf litter. Sciences of Soils 4(2):1432–9492. https://doi.org/10.1007/s10112-999-0002-x

Publisher's Note